Inelastic freeze-in

Saniya Heeba,[1,*] Tongyan Lin,[2,†] and Katelin Schutz[1,‡]

[1]*Department of Physics and Trottier Space Institute, McGill University, Montréal, Quebec H3A 2T8, Canada*

[2]*Department of Physics, University of California, San Diego, California 92093, USA*

(Received 14 August 2023; accepted 19 October 2023; published 8 November 2023)

Dark matter (DM) could be a nonthermal relic that freezes in from extremely weak, sub-Hubble annihilation and decay of Standard Model (SM) particles. The case of Dirac DM freezing in via a dark photon mediator is a well-studied benchmark for DM direct detection experiments. Here, we extend prior work to take into account the possibility that DM is pseudo-Dirac with a small mass splitting. If the mass splitting is greater than twice the electron mass but less than the dark photon mass, there will be distinct cosmological signatures. The excited state χ_2 is initially produced in equal abundance to the ground state χ_1. Due to the small couplings needed to explain the observed relic abundance, the excited state population can decay at late cosmological times, primarily via the three-body process $\chi_2 \to \chi_1 e^+ e^-$. This injects energetic electrons into the ambient environment, providing observable signatures involving big bang nucleosynthesis, cosmic microwave background spectral distortions and anisotropies, and the Lyman-α forest. Furthermore, the ground state particles that are populated from the three-body decay receive a velocity kick, with implications for DM clustering on small scales. Inelastic freeze-in thus gives a motivated decaying DM candidate, where the long lifetimes are connected to the relic abundance mechanism.

DOI: 10.1103/PhysRevD.108.095016

I. INTRODUCTION

The origins of dark matter (DM) in the early Universe remain an open question, with many possible thermal and nonthermal channels leaving a relic DM abundance that matches the observed present-day quantity $\Omega_c h^2 = 0.1200 \pm 0.0012$ [1]. If DM has a very small coupling to the Standard Model (SM) plasma such that interactions always occur at a rate below the Hubble expansion rate, then DM could be produced by the freeze-in mechanism. In this case, the DM is not in thermal equilibrium with the SM, and its density accumulates via rare annihilations and decays of particles in the SM thermal bath [2–4]. Many DM candidates, including sterile neutrinos and certain supersymmetric DM candidates, are naturally produced by the freeze-in mechanism [5–24]. Freeze-in is a rather general mechanism that can be realized in many models and produce the observed abundance of DM, provided the appropriate range of couplings [25].

The freeze-in mechanism naturally complements the possibility of a dark sector, where DM exists alongside other auxiliary particle content beyond the SM. For example, if there is a mediator that has a small coupling both to the SM and to the DM, then the small effective freeze-in couplings can be readily explained as originating from the product of two small numbers. A simple, technically natural example of such a mediator is a kinetically mixed dark photon [26]. In particular, freeze-in of Dirac fermions via dark photon interactions has emerged as a key benchmark model for direct detection experiments [27–29], where the same combination of couplings that explains the DM relic abundance also predicts the scattering cross section. The same freeze-in cross section can also be probed in cosmological searches [30], providing a motivated target in searches for DM-baryon interactions in the early universe [31,32].

Moving beyond this simple scenario, we note that when the dark gauge symmetry is broken, the Dirac fermions can split into two Majorana mass eigenstates and the couplings in this DM model are purely off-diagonal. This allows for inelastic processes that can be exothermic or endothermic, leading to markedly different behavior from the pure Dirac counterpart. The phenomenology of DM with inelastic interactions has been studied extensively, originally being proposed for its novel direct detection and astrophysical signatures [33–40]. For pseudo-Dirac DM, the mechanisms

*saniya.heeba@mcgill.ca
†tongyan@physics.ucsd.edu
‡katelin.schutz@mcgill.ca

for producing the relic abundance include the standard freeze-out production mechanism [41,42] as well as the resonant [43] and forbidden [44] regimes. This candidate was also studied in the freeze-in regime [45] for parameter space motivated by the subsequently excluded XENON1T excess [46,47]. More generally, the mass splitting leads to the possibility that the excited state can decay with long lifetimes. In the parameter space we explore in this work, the small couplings needed for freeze-in can lead to decays during relatively recent cosmological epochs. Inelastic freeze-in therefore provides a model target for cosmological searches for decaying DM, with a decay lifetime that is connected to the DM production mechanism.

In this paper, we focus on freeze-in of pseudo-Dirac DM via dark photon mediators. We work in the limit where the mediator is lighter than the DM, $m_{A'} < m_\chi$, which renders $m_{A'}$ as an irrelevant scale during freeze-in, making the required couplings insensitive to the mediator mass. Additionally, we will consider the regime where the A'—DM coupling is smaller than the A'—SM coupling, $g_\chi \lesssim e\epsilon$. Then the DM is dominantly produced through annihilations and decays of SM particles rather than freezing-in from a thermally populated dark sector. Freeze-in from the SM poses the most predictive scenario, which we shall subsequently refer to as "visible freeze-in" and which we will show can also be targeted by collider searches for the mediator in the $m_{A'} \sim 10$ MeV–10 GeV mass window.

Motivated by these considerations as well as by the possibility of complementary late-Universe phenomenology, we primarily consider DM in the mass range $m_\chi \sim 30$ MeV–1 TeV with mass-splittings $\delta > 2m_e$. With $\delta > 2m_e$, the standard lore (with some exceptions, e.g. [41,42]) for pseudo-Dirac DM in the freeze-out regime is that the excited state is efficiently depleted thermally in the early Universe. However, due to the small couplings in the freeze-in regime, the excited state does not necessarily get thermally de-populated and therefore there can be a metastable relic abundance of the excited state. We focus on the regime $\delta < m_{A'}$, which prevents the χ_2 from decaying rapidly via $\chi_2 \to \chi_1 A'$. For $\delta > 2m_e$, there will then be a late decay of the excited state to the ground state plus charged SM leptons, $\chi_2 \to \chi_1 \ell^+ \ell^-$. Meanwhile, for $\delta < 2m_e$ the lifetime of χ_2 would be many orders of magnitude longer than the age of the Universe since decays to neutrinos are suppressed by G_F^2 and phase space factors, and $\chi_2 \to \chi_1 + 3\gamma$ is also suppressed by powers of α_{em} and phase space factors [44]. For the couplings relevant to freeze-in, the decay $\chi_2 \to \chi_1 \ell^+ \ell^-$ can occur during cosmological epochs where the injection of energetic charged leptons can heat or ionize the baryons, causing an observable departure from the standard cosmology. Furthermore, the ground-state DM particle produced in the decay receives a velocity kick that would alter the formation of structure on small scales, which could be observable with probes of cosmological clustering.

The rest of this paper is organized as follows. In Sec. II, we review the model of pseudo-Dirac DM coupled to a kinetically mixed dark photon. We establish self-consistent theoretical motivations for considering our chosen parameter space that are complementary to the more phenomenological motivations described above. In Sec. III, we compute the freeze-in relic abundance, further establishing that the 50% of DM produced initially in the excited state is not immediately depleted by scattering processes. Specifically, we confirm that both $\chi_2 f \to \chi_1 f$ and $\chi_2\chi_2 \to \chi_1\chi_1$ are inefficient in the early Universe, ensuring a rich cosmological scenario where the excited state is metastable and can decay at later times. In Sec. IV we compute the differential decay width for the three-body decay, finding that most of the energy from the mass splitting ends up in the electrons and finding that the χ_1 gets a velocity kick of order $v \sim \delta/m_\chi$, resulting in half of the DM being "warmed up" after the excited state decays. In Sec. V, we explore existing cosmological constraints and future probes of the decay of metastable excited states from freeze-in (from both the injected electrons and the recoiling χ_1). Discussion and concluding remarks follow in Sec. VI.

II. MODEL AND PARAMETER SPACE

We consider a pseudo-Dirac DM model with two nearly mass-degenerate Majorana states χ_1 and χ_2, where the mass splitting is represented by $\delta = m_{\chi_2} - m_{\chi_1}$. This dark sector is coupled to the Standard Model through a massive dark photon, A', with dark gauge coupling g_χ. The dark photon kinetically mixes with the SM hypercharge with mixing strength ϵ, with the interaction Lagrangian,

$$\mathcal{L} \supset -\frac{\epsilon}{2} F'_{\mu\nu} F_Y^{\mu\nu} - i g_\chi A'_\mu \overline{\chi_2} \gamma^\mu \chi_1. \tag{1}$$

Rotating the fields to a basis with canonical kinetic terms, below the scale of electroweak symmetry breaking we obtain [48,49]

$$\mathcal{L} \supset -i\left(g_\chi A'_\mu + g_\chi \epsilon \sin\theta_W \frac{m_Z^2}{m_Z^2 - m_{A'}^2} Z_\mu\right) J^\mu_{\rm DM} + \frac{e\epsilon}{\cos\theta_W} \frac{m_{A'}^2}{m_Z^2 - m_{A'}^2} A'_\mu J_Y^\mu - e\epsilon \cos\theta_W \frac{m_Z^2}{m_Z^2 - m_{A'}^2} A'_\mu J^\mu_{\rm EM}, \tag{2}$$

where $m_{A'}$ is the dark photon mass, $J^\mu_{\rm EM(Y)}$ is the electromagnetic (hypercharge) SM current and $J^\mu_{\rm DM} = \bar{\chi}_2 \gamma^\mu \chi_1$ is the off-diagonal DM current. We consider purely off-diagonal interactions but note that models of inelastic DM with diagonal couplings are also possible [42,50,51].

A. Origin of dark sector masses and interactions

As a minimal setup for generating the dark sector masses and interactions, we consider a complex dark Higgs field,

Φ_D, with a dark charge of two that couples to a standard Dirac fermion Ψ with interactions [52,53]

$$\mathcal{L} = i\bar{\Psi}\not{D}\Psi - m_D\bar{\Psi}\Psi + (D_\mu\Phi_D)^\dagger(D^\mu\Phi_D) - y_\chi(\bar{\Psi}^C\Psi\Phi_D^* + \text{H.c.}) + V(\Phi_D), \tag{3}$$

where $D_\mu \equiv \partial_\mu - iqg_\chi A'_\mu$ is the covariant derivative, $q = 1(2)$ is the charge for $\Psi(\Phi_D)$, $V(\Phi_D)$ is the dark Higgs potential and C denotes charge conjugation. The vacuum expectation value (vev) of the dark Higgs, $\Phi_D = (v_D + h_D)/\sqrt{2}$ breaks the $U(1)_D$ symmetry, generating the dark photon mass. Additionally, the Yukawa interaction results in a Majorana mass term for the two components of Ψ. The corresponding fermion mass matrix is given by

$$\frac{1}{2}(\eta\ \xi)\begin{pmatrix} m_M & m_D \\ m_D & m_M \end{pmatrix}\begin{pmatrix}\eta \\ \xi\end{pmatrix} + \text{H.c.}, \tag{4}$$

with $m_M = \sqrt{2}y_\chi v_D$. This can be diagonalized to obtain two nearly mass-degenerate states, $\chi_1 = i(\eta - \xi)/\sqrt{2}$ and $\chi_2 = (\eta + \xi)/\sqrt{2}$. This change of basis gives the off-diagonal A' interaction in Eq. (1). In addition, there are interactions involving the dark Higgs, but we will be working in the limit of a heavy dark Higgs such that the interactions do not play an important role in the phenomenology.

In this scenario, we have the following relationships in the full theory:

$$m_{A'} = 2g_\chi v_D, \qquad \delta = 2\sqrt{2}y_\chi v_D$$
$$m_{\chi_{1,2}} = m_D \mp \sqrt{2}y_\chi v_D \qquad m_{h_D} = \sqrt{2\lambda_D}v_D. \tag{5}$$

Here λ_D is the dark Higgs quartic coupling. The splitting and overall mass scale of the DM depends on the relative size of the Majorana mass $\sqrt{2}y_\chi v_D$ to the Dirac mass m_D. Throughout the paper, we will generally work in the limit of $\delta \ll m_{\bar{\chi}}$, where $m_{\bar{\chi}} = (m_{\chi_1} + m_{\chi_2})/2$ can be considered as an average mass scale.

B. Parameter space

In this work, we will be primarily interested in the dark photon mass range $m_{A'} \in [10\ \text{MeV}, 10\ \text{GeV}]$, a benchmark for various ongoing and upcoming terrestrial searches (see for instance Fig. 2). Since we will work in the light mediator limit, $m_{A'} < m_{\bar{\chi}}$, we will consider $m_{\bar{\chi}} \sim$ 30 MeV–1 TeV. For $m_{\bar{\chi}} \lesssim 30$ MeV, strong bounds on $m_{A'}$ coming from accelerator searches imply that the light mediator limit is difficult to satisfy, whereas for $m_{\bar{\chi}} \gtrsim 1$ TeV, the electroweak phase transition may affect freeze-in production, which is beyond the scope of what we consider in this work. The parameter space we consider is also compatible with astrophysical constraints on dark photons from stellar energy loss [54], SN1987A [55], and cosmological constraints from big bang nucleosynthesis (BBN) [56].

Our focus is on visible freeze-in, where a single combination of couplings, ϵg_χ, determines both the DM relic abundance and late-Universe phenomenology. As we will show in the next section, in order to obtain the DM relic abundance in this scenario the typical couplings required are $\epsilon g_\chi \sim 10^{-11}$. For visible freeze-in, we also require $g_\chi \lesssim e\epsilon$, which implies small dark gauge couplings $g_\chi \lesssim 10^{-6}$. In the region of parameter space where g_χ is larger than ϵe, the production of DM would primarily be through dark photon fusion, which scales as g_χ^4, and destroys this tight connection between early-universe production and late-universe observables. Larger values of g_χ could also overproduce DM through dark photon fusion, although this requires further study accounting for in-medium effects [54]. Furthermore, keeping g_χ small is more interesting cosmologically because this prevents the depopulation of the excited state through $\chi_2\chi_2 \to \chi_1\chi_1$, as discussed in the next section. Motivated by this potential for a richer cosmology, we also focus on the parameter space where $\delta < m_{A'}$, which ensures that the excited state is cosmologically long-lived.

Finally, in order to isolate the effects of the pseudo-Dirac DM freeze-in, we require the dark Higgs to be sufficiently heavy to not meaningfully participate in any freeze-in dynamics or late-time interactions, with $m_{h_D} \gg m_{\bar{\chi}}, m_{A'}$. This requirement also has the effect of ensuring that in our parameter space, the dark Higgs is so heavy as to not be subject to strong stellar bounds [57]. Since the heaviest DM we consider has a mass of 1 TeV, $m_{h_D} \gg 1$ TeV. Together with the relationships in Eq. (5), $m_{h_D} \lesssim m_{A'}/g_\chi$, this suggests that $m_{A'}, m_{\bar{\chi}} \ll m_{h_D}$ over our entire parameter space for $g_\chi \lesssim 10^{-6}$, consistent with our assumptions.

III. EARLY UNIVERSE BEHAVIOR

A. Freeze-in production of DM

For $g_\chi \lesssim e\epsilon$, the dominant channels contributing to freeze-in are the annihilation of SM fermions, $f\bar{f} \to \chi_1\chi_2$, or Z-decays, $Z \to \chi_1\chi_2$. The latter process is most important in the mass range GeV $\lesssim 2m_{\bar{\chi}} < m_Z$. As noted in the previous section, dark photon fusion is a negligible DM production channel for the range of couplings we consider. We additionally note that purely finite-temperature production channels, such as plasmon decay to $\chi_1\chi_2$, are negligible for DM masses above ~1 MeV [29]. We also ignore the RG running of the couplings and the temperature corrections to the processes considered here. For production via Z-decays that happens at $T \sim m_Z/3$, thermal corrections to the Z-mass are much smaller than the vacuum value of the Z-mass [58]. For heavier DM, thermal corrections (e.g., thermal masses) may have an O(10%)

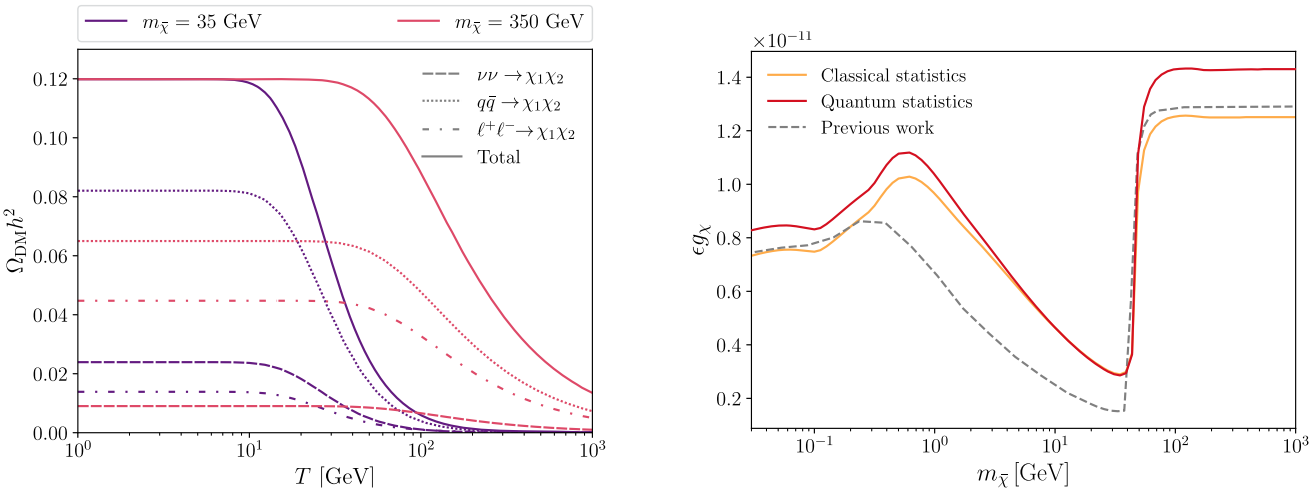

FIG. 1. Left: Evolution of the various contributions to the total DM abundance today, including the neutrino (dashed), quark (dotted) and charged lepton (dot-dashed) channels for $m_{\tilde{\chi}} = 35$ GeV (purple) and $m_{\tilde{\chi}} = 350$ GeV (pink). The masses are chosen to yield representative values of the freeze-in couplings that are maximally or minimally affected by Z-decays. Right: The coupling combination that reproduces the DM relic density in the light mediator limit. The result is shown as a function of the DM mass assuming classical (yellow) and quantum (red) statistics. The dashed gray line corresponds to results from previous work [3]. These results are independent of $m_{A'}$ and δ assuming $m_{A'} \ll m_{\tilde{\chi}}$, $m_{A'} \ll m_Z$, and $\delta \ll m_{\tilde{\chi}}$.

effect on the DM abundance [59] but will not change our results qualitatively.

Given the assumptions above, the DM number density can be obtained by solving the Boltzmann equation,

$$sHx\frac{\mathrm{d}Y_{\chi_1}}{\mathrm{d}x} = \langle\sigma v\rangle_{f\bar{f}\to\chi_1\chi_2} n_f^2 + \langle\Gamma\rangle_{Z\to\chi_1\chi_2} n_Z, \tag{6}$$

where $Y_{\chi_1} = n_{\chi_1}/s$ is the comoving number density of the ground or excited state, H is the Hubble rate, s is the entropy density, $x = m_{\tilde{\chi}}/T$, and the two terms on the right correspond to the thermally averaged annihilation and decay rates, respectively.

For $\delta \ll m_{A'}$ and $T \gg m_{\tilde{\chi}}$, the thermally averaged annihilation cross section above scales as $e^2\epsilon^2 g_\chi^2 \cos^2\theta_W/T^2$ in the light mediator limit, whereas the decay rate scales as $\epsilon^2 g_\chi^2 \sin^2\theta_W m_Z^2/(2T)$ for $T \gg m_Z$. The corresponding contributions to the total DM comoving number density can then be obtained by integrating Eq. (6) from $x \to 0$ to $x \to \infty$, giving

$$Y_{\chi_1}^{ff} \propto \frac{e^2\epsilon^2 g_\chi^2 \cos^2\theta_W M_{\rm Pl}}{m_{\tilde{\chi}}} \tag{7}$$

$$Y_{\chi_1}^{Z} \propto \frac{\epsilon^2 g_\chi^2 \sin^2\theta_W M_{\rm Pl}}{m_Z} \tag{8}$$

where $M_{\rm Pl}$ is the Planck mass.

For a more precise calculation of the DM production rate that includes the relevant relativistic spin statistics factors for particles in the initial state, we use the freeze-in routines of micrOMEGAs [60] with a pseudo-Dirac DM model implemented in CALcHEP [61]. The resulting DM production rate through various channels is plotted in the left panel of Fig. 1 for $m_{\tilde{\chi}} = 35$ GeV and $m_{\tilde{\chi}} = 350$ GeV. Note that micrOMEGAs includes the contribution from decays within the corresponding $2 \to 2$ processes in which the decaying particle can be produced on-shell (see Ref. [60] for details). This can be seen in the left panel of Fig. 1 as the difference in slope of the total production rate for $m_{\tilde{\chi}} = 35$ GeV, which gets a significant contribution from Z-decays, versus $m_{\tilde{\chi}} = 350$ GeV, which does not.

Summing up the various contributions gives us the total DM abundance,

$$\Omega_{\rm DM} = \frac{(Y_{\chi_1}^0 m_{\chi_1} + Y_{\chi_2}^0 m_{\chi_2})s^0}{\rho_c^0} \approx \frac{2Y_{\chi_1}^0 m_{\tilde{\chi}} s^0}{\rho_c^0}. \tag{9}$$

Here, ρ_c^0 and s^0 are the critical energy density and entropy density today. The last approximation comes from the fact that the ground and excited states are symmetrically produced because for $\delta \ll m_{\tilde{\chi}}$, the model effectively behaves as standard Dirac DM at the time of freeze-in when $T \gtrsim m_{\tilde{\chi}}$. Requiring that the final abundances matches the observed relic density [1] gives us the product of the couplings $g_\chi\epsilon$ as a function of the DM mass. The final result, $g_\chi\epsilon \sim O(10^{-11})$ in the DM mass range of interest, is plotted in Fig. 1 (right). The yellow line corresponds to solving the Boltzmann equation assuming a Maxwell-Boltzmann distribution for the particles in the initial state whereas the red line corresponds to a more accurate calculation using Fermi-Dirac and Bose-Einstein distributions as appropriate. For $2m_{\tilde{\chi}} > m_Z$, $g_\chi\epsilon$ is independent of the DM mass, which can also be inferred from Eqs. (7)–(9). We note that our results

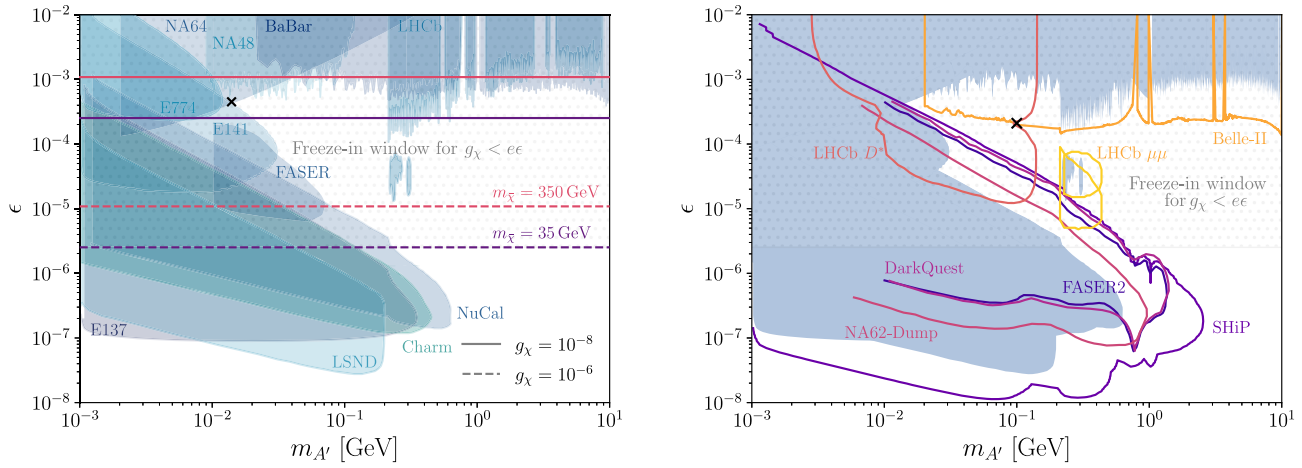

FIG. 2. Left: bounds on the freeze-in parameter space (dotted region) from beam dump and collider experiments. See [62–64] for a review. The horizontal lines show the values of ϵ for which we obtain the observed abundance of DM for $g_\chi = 10^{-8}$ (solid) and $g_\chi = 10^{-6}$ (dashed) and $m_{\tilde{\chi}} = 35$ GeV (purple) and $m_{\tilde{\chi}} = 350$ GeV (pink). In this paper, we focus on the window where $g_\chi < e\epsilon$ which gives visible freeze-in from SM particles (as opposed to from the dark sector). Right: projections from various experiments.

agree with those of [3] above a few hundred GeV and below 100 MeV, but differ by an $\mathcal{O}(1)$ factor around the Z resonance (dashed line in Fig. 1). This can be traced to a missing factor of $\tan\theta_W$ in Eq. (73) of [3].

In Fig. 2, we compare our freeze-in parameter space with accelerator searches for dark photons in the $\epsilon - m_{A'}$ plane. Assuming $g_\chi < 10^{-6}$, there is a minimum kinetic mixing for freeze-in to produce the observed relic abundance. This minimum on the freeze-in window is given by the dashed lines for $m_{\tilde{\chi}} = 35$ GeV and $m_{\tilde{\chi}} = 350$ GeV. As noted above, for DM with masses around ~10 GeV, the primary mode of production occurs via Z-decays, so smaller values of ϵg_χ produce the observed relic DM density compared to the $m_{\tilde{\chi}} = 350$ GeV benchmark. Additionally, for $m_{A'}, \delta \ll m_{\tilde{\chi}}$, the DM freeze-in abundance is independent of the dark photon mass and the mass-splitting. The shaded regions of Fig. 2 show bounds (left) and projections (right) from various fixed-target, beam dump, collider and neutrino experiments on a kinetically mixed dark photon [62–64].

Collider searches for inelastic DM excited states (rather than the mediator) are possible [65–67]; however, these searches have focused on dark photons with $m_{A'} > m_{\chi_1} + m_{\chi_2}$, as motivated by the larger production cross section and the benchmark of the visible (rather than dark sector) freeze-out thermal history. Such collider searches do not constrain the freeze-in scenario described in this work because we consider lighter mediators $m_{A'} < m_{\chi_1} + m_{\chi_2}$, the production cross sections are suppressed by the tiny freeze-in couplings, and the excited state is cosmologically long-lived, beyond the range of timescales that can be probed at colliders.

We also note that there may be direct detection signatures of the cosmologically populated excited state (rather than being produced in a collider) if it has a lifetime that is longer than the age of the Universe. This is possible in parts of the parameter space due to the small mass splitting and small freeze-in couplings, and is trivially true if the mass splitting drops below the ~MeV two electron threshold. This would lead to a situation where the relic DM excited state can potentially down-scatter in terrestrial experiments and deposit energy. Traditional direct detection experiments are sensitive to a range of energy depositions that are below the mass splittings we consider in this work, but neutrino experiments could have sensitivity in the appropriate energy range. Despite the large exposures provided by neutrino experiments, a preliminary estimate suggests that due to the very small couplings relevant for freeze-in, the expected number of observed down-scattering events is much less than unity. Another avenue to produce signatures at direct detection experiments is to upscatter the ground state through interactions with cosmic rays followed by downscattering in the detector [68]. However, Ref. [69] showed that inelastic up-scattered DM can be used to constrain DM-nucleon couplings as small as $g_N g_\chi \sim 10^{-4}$, which is much larger than the freeze-in couplings we consider in this work. Therefore, we find no meaningful possibility of probing this parameter space via direct detection.

B. Scattering processes

Although the ground and excited states are populated equally by freeze-in, scattering processes may change their relative number density after production. In this section, we consider processes that convert χ_2 to χ_1 (and vice versa). If efficient, these reactions can establish chemical equilibrium in the dark sector with the Please note that as per PRD style, the bullets in the bulleted lists have been changed to roman lowercase letters.ground and excited state densities related

by $n_{\chi_2} \sim e^{-\delta/T_\chi} n_{\chi_1}$, where T_χ is the dark sector temperature. Accordingly, any interactions that keep the dark sector in chemical equilibrium can deplete the χ_2 density for $T_\chi \lesssim \delta$ [41,45]. We show below that these processes are negligible in our parameter space of interest.

(i) Coscattering off of SM fermions: $\chi_1 f \leftrightarrow \chi_2 f$. The dominant coscattering channel is with electrons. The rate of this process per DM particle, $\Gamma = n_e \sigma v$, scales as $e^2\epsilon^2 \cos^2\theta_W g_\chi^2 T^3/m_{A'}^2$ in the high-temperature limit, and therefore could become efficient with $\Gamma > H$ at early times. However, at such large temperatures, the number densities of $\chi_{1,2}$ are negligible compared to the final freeze-in relic abundance. A better metric for comparison is therefore the rate normalized with the fractional comoving abundance of dark matter, $\tilde{\Gamma} = (Y_{\rm DM}(T)/Y^0_{\rm DM})\Gamma$, where $Y^0_{\rm DM}$ is the total comoving abundance of DM today. The rescaling by $Y_{\rm DM}(T)/Y^0_{\rm DM}$ captures the fact that DM produced by freeze-in at early times (which could come into equilibrium with the SM) would be a small subcomponent and the majority of the total DM could be produced well after coscattering becomes inactive. Simply comparing Γ to the Hubble expansion rate would not capture the fact that any early thermalization would not significantly affect the majority of the DM, whose phase space distribution would be determined by the freeze-in production channel rather than by coscattering. In the limit $Y_{\rm DM}(T)/Y^0_{\rm DM} \to 1$, when most of the DM has been produced, our comparison of the normalized coscattering rate $\tilde{\Gamma}$ with H reduces to the usual comparison involving Γ.

In Fig. 3, we plot the normalized coscattering rate of DM with electrons as a function of temperature for different values of $m_{\tilde{\chi}}, m_{A'}$, and the couplings that produce the observed DM abundance. The requirement that this rate be sub-Hubble at freeze-in, $T \sim m_{\tilde{\chi}}$, results in a lower bound on the dark photon mass for a given DM mass. Using our estimate of Γ gives a rough bound of $m_{A'} \gtrsim e\epsilon \cos\theta_W g_\chi \sqrt{M_{\rm pl} m_{\tilde{\chi}}} \sim 0.29\ {\rm GeV}\sqrt{m_{\tilde{\chi}}/{\rm TeV}}$. To determine a more careful bound, as well as to show the rate in Fig. 3, we calculate the $\chi_1 f \to \chi_2 f$ cross section numerically using CALcHEP. This gives $m_{A'} > 28$ MeV for $m_{\tilde{\chi}} = 350$ GeV and $m_{A'} > 48$ MeV for $m_{\tilde{\chi}} = 1$ TeV, somewhat lower than the analytic estimate. We emphasize that this bound should be understood as a consistency check for our requirement that the vast majority of DM is never in equilibrium with the SM, since this could lead to thermal depletion of the excited state. In the parameter space where this requirement does not hold, the Boltzmann equation we use to compute the freeze-in relic abundance would no longer be accurate. One would then have to solve fully coupled Boltzmann equations for the ground and excited states (potentially at the level of the phase space) to accurately calculate the DM abundance, similar to Refs. [50,70], which is beyond the scope of this work.

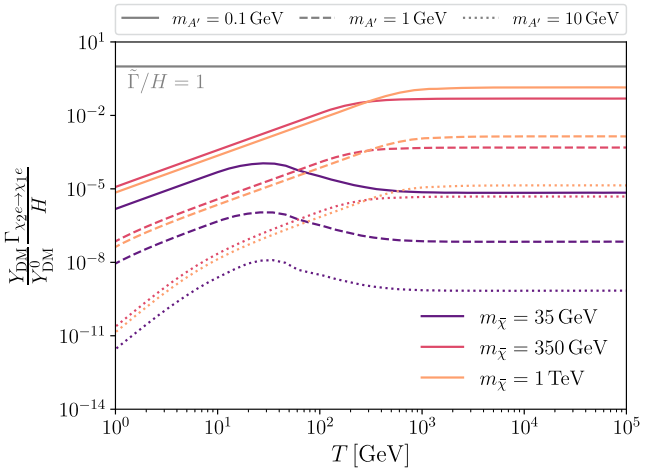

FIG. 3. The normalized coscattering rate of DM with electrons, $\chi_1 e \leftrightarrow \chi_2 e$, compared to the Hubble rate as a function of temperature for different values of $m_{\tilde{\chi}}$ and $m_{A'}$. The couplings are chosen to satisfy the DM relic abundance. See text for details.

(ii) Up/down-scattering: $\chi_1\chi_1 \leftrightarrow \chi_2\chi_2$. The cross sections for this process have been studied in [71] in the non-relativistic limit. In the parameter space we consider, $m_{\chi_1}\alpha_\chi \ll m_{A'}$ and therefore we can use the analytic results in the Born approximation derived in [71]:

$$\sigma_{\chi_1\chi_1\to\chi_2\chi_2} = \frac{4\pi\alpha_\chi^2 m_{\chi_1}^2 \sqrt{1-\frac{2\delta}{m_{\chi_1}v^2}}}{m_{A'}^4\left[\left(1-\frac{2\delta m_{\chi_1}}{m_{A'}^2}\right)^2 + \frac{4m_{\chi_1}^2 v^2}{m_{A'}^2}\right]} \tag{10}$$

$$\sigma_{\chi_2\chi_2\to\chi_1\chi_1} = \frac{\sigma_{\chi_1\chi_1\to\chi_2\chi_2}}{\left(1-\frac{2\delta}{m_{\chi_1}v^2}\right)}, \tag{11}$$

where v is the velocity of either of the DM particles in the center of mass frame. For DM produced via freeze-in, the momentum is inherited from the SM thermal bath with a typical momenta of T and velocity $v \sim T/m_\chi$. Substituting for v allows us to then calculate the corresponding rates, $n_{\chi_{1,2}}\sigma_{\chi_1\chi_1\leftrightarrow\chi_2\chi_2}v$. The rate can also be analytically estimated as $\Gamma \sim 10^{-8}\ {\rm GeV} \times \alpha_\chi^2 T^4/(m_{A'}^4 + 4m_{A'}^2 T^2)$, where the DM number density is obtained by scaling back its present day abundance, $\rho_{\rm DM}(T) \sim \rho^0_{\rm DM}(T/T_0)^3$. For DM in our mass range, this corresponds to an upper bound on $\alpha_\chi \lesssim 10^{-7}$ at the temperatures relevant for freeze-in. As mentioned

above, we are interested in the regime $g_\chi \lesssim e\epsilon \sim 10^{-6}$, and therefore in our parameter space of interest, these scattering processes are always sub-Hubble. We validate the above estimates with numerical calculations of the full cross section using CALCHEP, since for $T \gtrsim m_{\bar{\chi}}$ the approximations in [71] are no longer valid. The full results in the nonrelativistic limit are closely approximated by the expressions given in Eqs. (10) and (11). Note that in our model, up- and down-scattering can also take place through a Z in the t-channel, and we have checked numerically that the contribution from this diagram is negligible.

In summary, the dark sector never enters into chemical or kinetic equilibrium with itself or with the SM. Therefore the comoving number densities of the ground and excited states are the same as their values at the end of freeze-in production. The fact that 50% of DM is present in the excited state until later times is necessary for having cosmological signatures.

IV. OUT-OF-EQUILIBRIUM DECAYS

Due to the small freeze-in couplings required to yield the observed DM relic abundance, there is no substantial DM annihilation rate to the SM via processes such as $\chi_2\chi_1 \to f\bar{f}$. At the time of recombination, this rate is well below CMB bounds on DM annihilation [1,72]. However, the small freeze-in couplings can lead to a long lifetime for the excited DM state, with the result that 50% of the DM is decaying in the late universe. The signatures of the late decay depend on the channel as well as the kinematics.

If $\delta < 2m_e$, the excited state can only decay into $\chi_1\nu\bar{\nu}$ and $\chi_1 + 3\gamma$. The rates for these processes are suppressed by a factor of G_F^2 and an electron loop respectively, as well as phase space factors, making the excited state extremely long-lived on cosmological timescales (see Appendix B1 of [44]). On the other hand, for $\delta > 2m_e$, the excited state can decay into charged leptons, $\chi_2 \to \chi_1\ell^+\ell^-$ with the dominant decay channels being electrons ($\delta > 2m_e$) and muons ($\delta > 2m_\mu$) for MeV-GeV scale A'. To a very good approximation, above the decay threshold the partial decay width is independent of the lepton mass and is given by,

$$\Gamma_{\chi_2\to\chi_1\ell^+\ell^-} \approx \frac{g_\chi^2(e\epsilon\cos\theta_W)^2}{60\pi^3}\frac{\delta^5}{m_{A'}^4}, \tag{12}$$

corresponding to a decay timescale of

$$\tau \sim 1.3\times 10^7\ \mathrm{s}\left(\frac{\epsilon g_\chi}{10^{-11}}\right)^{-2}\left(\frac{\delta}{100\ \mathrm{MeV}}\right)^{-5}\left(\frac{1\ \mathrm{GeV}}{m_{A'}}\right)^{-4}. \tag{13}$$

This decay injects energetic leptons into the SM plasma and provides a velocity kick to the DM at times that are relevant to cosmological observables. Depending on the phase space of the decay products and the decay time, different cosmological probes can be used to hunt for signatures of this model.

In order to calculate the phase space, we start by assuming that the relic population of χ_2 is effectively at rest during the epochs relevant for cosmological observables. The consistency of this assumption is validated below. The phase space for the three-body decay is given by

$$\int \mathrm{d}\Gamma = \frac{1}{m_{\chi_2}}\int \frac{\mathrm{đ}^3 p_{\chi_1}}{2E_{\chi_1}}\frac{\mathrm{đ}^3 p_{\ell^+}}{2E_2}\frac{\mathrm{đ}^3 p_{\ell^-}}{2E_3}|M|^2_{\chi_2\to\chi_1\ell^+\ell^-} \times (2\pi)^4\delta^4(p_{\chi_2} - p_{\chi_1} - p_{\ell^+} - p_{\ell^-}), \tag{14}$$

where $\mathrm{đ}^3 p_i = \mathrm{d}^3\vec{p}_i/(2\pi)^3$ and the matrix element for the decay is

$$|M|^2_{\chi_2\to\chi_1\ell^+\ell^-} = \frac{16(e\epsilon g_\chi\cos\theta_W)^2}{((p_{\chi_2}-p_{\chi_1})^2 - m_{A'}^2)^2}[m_\ell^2(p_{\chi_2}\cdot p_{\chi_1}) - m_{\chi_1}m_{\chi_2}(p_{\ell^+}\cdot p_{\ell^-}) + (p_{\chi_1}\cdot p_{\ell^-})(p_{\chi_2}\cdot p_{\ell^+}) + (p_{\chi_2}\cdot p_{\ell^-})(p_{\chi_1}\cdot p_{\ell^+}) - 2m_\ell^2 m_{\chi_1}m_{\chi_2}]. \tag{15}$$

In the rest frame of χ_2, energy-momentum conversation dictates that the momentum of χ_1 is equal and opposite to the net momentum of the $\ell^+\ell^-$ pair,

$$|\vec{p}_{\chi_1}| = \frac{m_{\chi_2}}{2}\sqrt{1 - \frac{2(m_{\chi_1}^2 + s_{23})}{m_{\chi_2}^2} + \frac{(m_{\chi_1}^2 - s_{23})^2}{m_{\chi_2}^4}}, \tag{16}$$

where $\sqrt{s_{23}}$ is the effective mass of the lepton pair, $\sqrt{s_{23}} = \sqrt{E_{\ell^+\ell^-}^2 - \vec{p}_{\chi_1}^2}$ for net lepton pair momentum $\vec{p}_{\ell^+\ell^-} = -\vec{p}_{\chi_1}$. Then, using the standard treatment for a three-body phase space [73], we can write the partial decay width as

$$\int \mathrm{d}\Gamma = \frac{1}{128\pi^2 m_{\chi_2}}\int \frac{ds_{23}}{2\pi} \times \sqrt{1 - \frac{2(m_{\chi_1}^2 + s_{23})}{m_{\chi_2}^2} + \frac{(m_{\chi_1}^2 - s_{23})^2}{m_{\chi_2}^4}} \times \sqrt{1 - \frac{4m_\ell^2}{s_{23}}}|\tilde{M}(s_{23})|^2. \tag{17}$$

Here $|\tilde{M}|^2$ is the matrix element squared integrated over all angles in the rest frame of s_{23}. Equation (17) can then be used to obtain a differential decay rate in either $|\vec{p}_{\chi_1}|$ or in $E_{\ell^+\ell^-}$ using the relationships with s_{23} above.

We can parametrize the effect of this decay on the dark and visible sectors in terms of the average kick velocity to the χ_1 produced in the decay, $\langle v_{\mathrm{kick}}\rangle$, and the average energy carried by the lepton pair, $\langle E_{\ell^+\ell^-}\rangle$. We define each of these quantities as

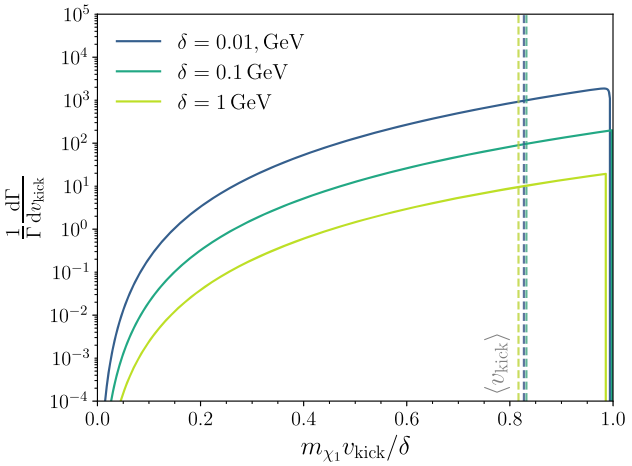

FIG. 4. The differential decay width as a function of a normalized kick velocity, $m_{\chi_1} v_{\rm kick}/\delta$, for different values of δ. For concreteness, lines are shown with $m_{\chi_1} = 35$ GeV; results with other m_{χ_1} are very similar. The dashed lines correspond to the average kick velocity, $\langle v_{\rm kick} \rangle$.

$$\langle v_{\rm kick} \rangle = \frac{1}{\Gamma} \int dv_{\chi_1} \frac{d\Gamma}{dv_{\chi_1}} \times v_{\chi_1}, \tag{18}$$

$$\langle E_{\ell^+\ell^-} \rangle = \frac{1}{\Gamma} \int dE_{\ell^+\ell^-} \frac{d\Gamma}{dE_{\ell^+\ell^-}} \times E_{\ell^+\ell^-}. \tag{19}$$

Since $s_{23} \in [4m_\ell^2, \delta^2]$, the limits of the integrals above are given by

$$0 \leq |\vec{p}_{\chi_1}| \leq \frac{1}{2m_{\chi_2}} \sqrt{(\delta^2 - 4m_\ell^2)((m_{\chi_1} + m_{\chi_2})^2 - 4m_\ell^2)} \tag{20}$$

$$\frac{\delta(m_{\chi_1} + m_{\chi_2}) + 4m_\ell^2}{2m_{\chi_2}} \leq E_{\ell^+\ell^-} \leq \delta. \tag{21}$$

In Fig. 4, we plot the normalized differential decay width as a function of the velocity kick given to χ_1 for $m_{\chi_1} = 35$ GeV, $m_{A'} = m_{\chi_1}/10$ and different values of δ. The dashed lines represent the average value of the kick velocity. Note that although we plot the curves for specific values of m_{χ_1} and $m_{A'}$, the normalization of the axes ensures that, for a given δ, any value of $m_{\chi_1}, m_{A'}$ will essentially map on to the same lines. Additionally, Eq. (21) implies that the energy transferred to the leptons is sharply peaked around the mass splitting.

It follows that the average kick velocity and the average energy transferred are given by,

$$\langle v_{\rm kick} \rangle \approx \frac{\delta}{m_{\chi_1}}, \qquad \langle E_{\ell^+\ell^-} \rangle \approx \delta. \tag{22}$$

These values are derived in the rest frame of χ_2, and will be essentially the same in the comoving frame if the typical speed of χ_2 is much smaller than $v_{\rm kick}$ at the time of decay. Freeze-in ends when the SM temperature $T \sim m_{\bar{\chi}}$ and the χ_2 has a typical momentum of $p_{\chi_2} \sim T$ at this time. Since the DM is not in kinetic equilibrium, the momentum redshifts along with the SM thermal bath temperature and at late times $v_{\chi_2} \sim T/m_{\chi_2}$. This residual speed at the time of decay will be smaller than $v_{\rm kick}$ as long as $T \ll \delta$, which is a valid approximation for the cosmological observables that we consider in this work. We can now apply the distributions derived above to a range of interesting consequences for cosmological observables in the following Section.

V. COSMOLOGICAL SIGNATURES

The out-of-equilibrium decays of the metastable excited state can have observable implications in ongoing and future cosmological probes. In this section, we focus on the two complementary classes of signatures coming from (1) energy injection into the baryonic sector and (2) suppressing structure formation on small scales due to streaming effects.

A. Energy injection from charged lepton pairs

As shown in the previous section, the e^+e^- pairs (or $\mu^+\mu^-$ pairs, if the mass splitting is above threshold) from the three-body decay get an $\mathcal{O}(1)$ fraction of the energy available from the mass splitting. These charged particles can subsequently deposit their energy into the photon-baryon plasma or intergalactic medium (IGM), causing ionization and heating. The efficiency of these effects depends on the energy of the electrons (or other SM particles) and ambient properties of the plasma or IGM, and is captured via a parameter $f_{\rm eff}(z)$, defined as the ratio between the rate of injected and deposited energy density,

$$\frac{dE_{\rm dep}}{dVdt} = f_{\rm eff}(z) \frac{dE_{\rm inj}}{dVdt} \tag{23}$$

$$= f_{\rm eff}(z) \frac{\rho_{\rm DM}(z)\delta}{2m_{\bar{\chi}}} \Gamma e^{-\Gamma t}. \tag{24}$$

In the second line, we have used the fact that half of the DM density is initially in the excited state and essentially all of the energy from the mass splitting goes into the leptons. Here $\Gamma = \Gamma_{\chi_2 \to \chi_1 \ell^+\ell^-}$. The efficiency $f_{\rm eff}(z)$ depends on the redshift and energy spectrum of injected particles. Depending on the redshift when the decay occurs, this energy deposition can alter BBN, the spectrum of cosmic microwave background (CMB) photons, CMB anisotropies, and Lyman-α forest measurements. There is also a possibility for 21 cm signatures in the future [35,74–76], pending an improved understanding of the relevant baryonic astrophysics and observational systematics. Assuming coupling constants fixed by freeze-in to produce the DM relic abundance, we can then place bounds in the

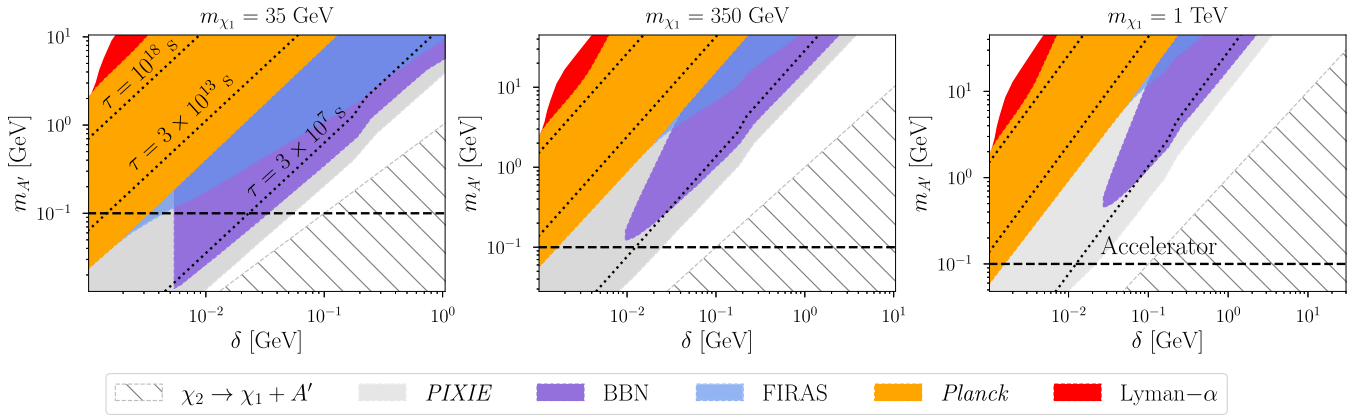

FIG. 5. Constraints and forecast sensitivity for the dark photon mass and DM mass splitting at different DM masses corresponding to $m_{\chi_1} = 35$ GeV, 350 GeV, and 1 TeV (left, middle, and right panels). For all constraints, it is assumed that the coupling combination $g_\chi \epsilon$ is fixed by saturating the DM relic abundance with freeze-in. In the hatched gray region, the excited state is not cosmologically relevant because it decays extremely rapidly (right after freeze-in) via $\chi_2 \to A'\chi_1$. The mass splitting is shown for values above the ∼MeV electron production threshold for three-body decay. Meanwhile, the depicted dark photon masses range from the minimum allowed by beam dump and collider experiments (shown as a black × in the left panel of Fig. 2) or alternatively the minimum $m_{A'}$ from becoming cosmologically relevant as shown in Fig. 3. The maximum value of $m_{A'}$ depicted goes up to $m_{A'} = m_{\chi_1}/3$, since we focus on the parameter region with $m_{A'} \ll m_{\chi_1}$, but for heavier DM masses we also ensure that $m_{A'} \ll m_Z$ which was an assumption made in the freeze-in analysis. The dashed horizontal line represents the minimum $m_{A'}$ that can be accessed in the near future with beam dump and collider experiments in the window of visible freeze-in couplings, shown as a black × in the right panel of Fig. 2. Meanwhile, the diagonal dotted lines correspond to contours of constant χ_2 lifetime for a few representative values (corresponding roughly to (i) the age of the Universe, (ii) shortly after recombination, and (iii) one year after the big bang, from left to right).

parameter space of $m_{\bar{\chi}}, m_{A'}$, and δ. All of the bounds and forecast sensitivities are summarized in Fig. 5.

For decay lifetimes $\tau \lesssim 10^{12}$ s, BBN currently provides the tightest constraints on decaying DM [77–80]. At times prior to recombination, energy injected in the form of e^+e^- pairs is approximately instantly deposited into the plasma and $f_{\rm eff} \approx 1$. The energy injection from DM three-body decays can therefore enhance the dissociation of light elements produced during BBN. The yields of these elements are very sensitive to changes in the ambient environment during and after BBN, and thus the agreement of the measured yields with the ΛCDM prediction can be used to constrain DM decay at early times. Note that the dissociation only proceeds if the spectrum of injected electron energies has support above the ∼3 MeV energy threshold for breaking apart light nuclei. For our model, the *combined* electron-positron energy is effectively monochromatic, but the energy of each of the individual particles can vary. This ∼3 MeV threshold can have a large impact on the bounds when δ is near the MeV-scale. For instance, Ref. [79] bounds the total fraction of DM energy injected into the electromagnetic sector assuming electrons are injected with energy above 10 MeV, while Ref. [80] finds that there is a large impact on the limits when the energy of the electrons injected is at the ∼10 MeV scale. Without doing a re-analysis of BBN bounds with our specific electron spectrum, we conservatively apply the BBN constraints of Ref. [79] when $\delta > 6$ MeV and note that it is possible the bound extends slightly below this. The application of this cut is apparent in the left panel of Fig 5, where the shape of the BBN bound differs from the other panels. In all, we find that due to the dependence of the decay rate on δ and $m_{A'}$, BBN is currently able to exclude a large swatch of parameter space for pseudo-Dirac freeze-in.

When the decay occurs with a range of decay lifetimes 10^7 s $\lesssim \tau \lesssim 10^{13}$ s, the energy injection heats the plasma which alters the spectrum of CMB photons. The spectrum does not have time to rethermalize if the energy injection happens below redshift $z \sim 10^6$, corresponding to $\tau \sim 10^7$ s or around 1 year after the big bang. This causes a spectral distortion where the CMB spectrum deviates from a perfect blackbody [81]. During the spectral distortion window, charged particles deposit their energy into the plasma almost instantaneously in a way that is insensitive to the energy spectrum of injected electrons, so again $f_{\rm eff} \approx 1$ with no strong dependence on δ. This is the so-called "on-the-spot" approximation for energy deposition, which is a good approximation for $z \gtrsim 1000$ [82,83]. A more precise value for $f_{\rm eff}(z)$ can be calculated by using tools such as DARKHISTORY [84] or EXOCLASS [85].

There are strong bounds on deviations of the CMB spectrum from a perfect blackbody [86,87], which can then be translated to bounds on a fraction of the DM decaying to energetic electrons [82]. These bounds as applied to our parameter space are shown in Fig. 5 in the region labeled "FIRAS," in reference to the Far Infrared Absolute Spectrometer aboard the Cosmic Background Explorer

(COBE) [86]. While current spectral distortion limits are not very competitive with other probes in the relevant decay lifetime window (almost everything excluded by FIRAS is already excluded by BBN), there would be a large improvement in sensitivity to our parameter space [82,88] with the proposed Primordial Inflation Explorer (PIXIE) mission [89], as shown in the light gray region in Fig. 5 labeled "PIXIE."

At times during and after recombination, $\tau \gtrsim 10^{13}$ s, the injection of energetic electrons can partly ionize and heat the IGM. In ΛCDM, the IGM is almost completely neutral after recombination and the photons free-stream to good approximation; ionization of the IGM due to DM decay will cause CMB photons to rescatter, smearing out the anisotropies. Strong bounds on the ionization fraction of the IGM from Planck anisotropy measurements constrain the deposition of ionization energy, which can be translated to a constraint on decaying DM. Similarly, there is a possibility that energy injection will heat the IGM during epochs around $z \sim 5$, where the Lyman-α forest of atomic absorption lines constrains the IGM temperature. Given a measurement of this temperature, one can exclude processes which would further heat the IGM, allowing a constraint to be set on the DM decay lifetime. For both ionization and heating, $f_{\rm eff}$ can vary substantially as a function of the injected energy spectrum, species, and redshift of injection, requiring a careful analysis involving the use of specialized codes which self-consistently take into account the effects of DM decay on the thermal history of the IGM, including backreactions [84,85]. We leave such an analysis as applied to our model for future work, and note that because our charged particle spectra are not monoenergetic, we are only able to estimate the corresponding limits.

In order to estimate the limits on our parameter space, for decay lifetimes near the time of recombination we apply the bounds of Ref. [82]. This work constrained the fraction of DM decaying as a function of decay lifetime assuming $f_{\rm eff} = 1$, which is a good approximation during and before recombination. When translated to our parameter space we find that the resulting limit is not very sensitive to this assumption about $f_{\rm eff}$. At late times well after recombination, however, $f_{\rm eff}$ can vary considerably so we apply the bounds from Ref. [90] for CMB anisotropies and Ref. [91] for the Lyman-α forest which solved for the deposition efficiency in a self-consistent way. Instead of constraining the fraction of DM decaying as a function of decay lifetime, as was done in Ref. [82], these works instead constrain the DM decay lifetime as a function of DM mass, and the effects of the energy spectrum on $f_{\rm eff}$ cause this limit to vary considerably for different DM masses. Both of those works considered DM decay where the electron energy injection spectrum is centered at half the DM mass, so we translate their bounds by matching their DM mass with our mass splitting, noting that this translation is only an estimate because our electron energy spectrum is broad while theirs is effectively a mono-energetic line. Moreover, the energy density available from the DM mass splitting is a small fraction of the total energy density of the DM. We therefore estimate the constraint on our parameter space by rescaling the decay rate to account for the lower energy density available in the mass splitting so that the *total* energy injected into the IGM is the same. Concretely, we re-scale the lifetime bounds of Refs. [90] and [84] by $\delta/2m_{\tilde{\chi}}$, as in Eq. (24). This re-scaling is supported by works that consider a subcomponent of DM decaying rather than looking at all of the DM having a particular decay lifetime [79,82,90]. The resulting estimated limits on our parameter space, combining early and late times, are shown as shaded regions in Fig. 5.

For lifetimes comparable to the age of the Universe, there can also be constraints on decaying DM from indirect searches for the decay products, e.g., with x-ray and gamma ray searches [92–95] which generally are weaker than cosmological constraints from the IGM in the parameter space of interest. One exception to this is the search for cosmic ray electrons and positrons directly from the decay; these particles cannot be detected from inside the solar system due to shielding from the solar magnetic field, but they can be observed by Voyager I [96], which has crossed the heliopause. The resulting limits on decaying DM of Ref. [97] are stronger than cosmological ones for mass splittings greater than $\delta \gtrsim 20$ keV, however when the corresponding lifetimes are mapped onto our parameter space, the values of $m_{A'}$ are too large for the analysis in this work to be valid. Therefore, these limits do not appear in Fig. 5 as the relevant parameter space probed by indirect detection searches is already excluded by cosmological ones.

B. Free-streaming of the ground state

As shown in the previous section, as the relic 50% of DM in the excited state decays, the resulting ground state daughter particle receives a velocity kick with a recoil spectrum peaked near $v \sim \delta/m_\chi$. As a result, the 50% of the DM that was born in the ground state behaves as cold DM, while the other 50% that gets produced from the decay can undergo some free streaming, similar to warm DM (WDM) or neutrinos. This effect has been previously studied in detail in situations where all of the DM decays via a two-body process to the ground state and a light degree of freedom [98,99]. In this section, we instead estimate the free-streaming length for the ground state population produced via three-body decays, with a more detailed study of structure formation in this model left to future work. Based on our estimates, we find untested parameter space to be within the reach of current probes of structure formation on small scales, and potentially of interest for future probes.

To estimate the scale of suppression of the transfer function relevant for the matter power spectrum, we employ the commonly used metric of the free-streaming length.

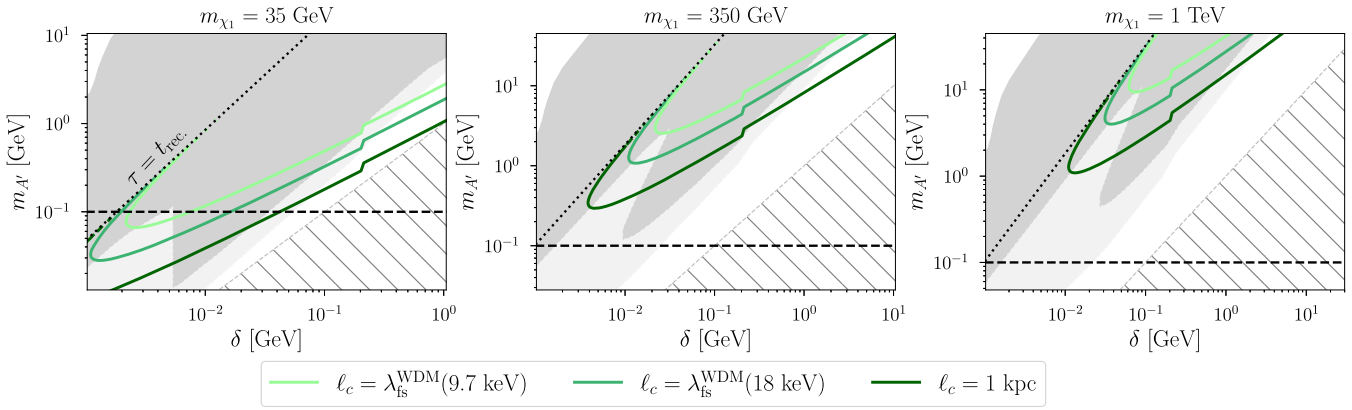

FIG. 6. The same parameter space as Fig. 5 but showing the complementarity with probes of structure formation. Existing cosmological constraints from Fig. 5 are shown here as dark gray regions, while the forecast for PIXIE is shown in light grey. The green lines correspond to parameters that give a decay timescale and velocity kick that will yield a free streaming length $\ell_c(t_{\rm rec})$, as estimated in Eq. (25), equivalent to that of WDM at a given mass.

We estimate this by assuming that the DM gets a physical velocity kick $v_{\rm kick}$ at a time set by the lifetime τ and that it free-streams with a Hubble-damped velocity. Ignoring any motion prior to the kick, the co-moving distance traveled by the DM by some later time t is

$$\ell_c(t) = \int_\tau^t \frac{v_d a(\tau) dt'}{a(t')^2} = \int_{z(t)}^{z(\tau)} \frac{v_d (1+z) dz}{H(z)(1+z(\tau))} \qquad (25)$$

where $H(z) = H_0\sqrt{\Omega_\Lambda + \Omega_m(1+z)^3 + \Omega_r(1+z)^4}$. For the energy densities and present-day Hubble parameter, we take the best-fit values from Planck 2018 [1]. Note that the approximation of free-streaming is not a good one for times long after matter-radiation equality (i.e., deep in the matter-dominated era) because of the onset of structure formation leading to gradients in the gravitational potential. In order to be conservative in our estimate of the comoving free streaming length today, we consider the free-streaming length at the time of recombination, $\ell_c(t_{\rm rec})$. This means that our estimate only applies in the parameter space to the right of the contour of constant $\tau = t_{\rm rec}$, as shown in Fig. 6.

In order to estimate the sensitivity of probes of structure formation in our parameter space, we equate $\ell_c(t_{\rm rec})$ with the free-streaming length of the well-studied WDM model, $\lambda_{\rm fs}^{\rm WDM} = 0.07 \times (m_{\rm WDM}/1\ {\rm keV})^{-1.11}$ Mpc for a Hubble parameter of $H_0 = 70$ km/s/Mpc [100–102]. This free-streaming length maps onto the transfer function for the matter power spectrum, as determined via Boltzmann solvers, and leaves an imprint on the subsequent formation of structure on small scales. There are many probes of structure on small scales in linear and nonlinear regimes, including the Lyman-α forest [103–105], the detection of low-mass subhalos with galaxy surveys [106,107], gravitational lensing and perturbations to stellar streams induced by subhalos [108–111], and eventually 21 cm cosmology [112]. Combining these probes can also help to break degeneracies and strengthen bounds [113,114]; in particular, Ref. [114] was able to set a relatively aggressive bound of $m_{\rm WDM} > 9.7$ keV at 95% confidence.

In Fig. 6 we show the parameter points that yield an estimated free-streaming length for pseudo-Dirac freeze-in which matches that of a 9.7 keV WDM model. We use the free-streaming length only to estimate the parameter space where there might be observable impacts on structure formation, and our estimate should not be taken as a constraint since the results of Ref. [114] do not apply directly to this scenario. Scenarios with mixed warm and cold dark matter [115–117] are more similar to the one considered here, but still differ since in this case the decay of DM induces a non-trivial time dependence to the phase space. A more detailed analysis is therefore necessary to derive a constraint, which will be the subject of future work.

In the near future, the Vera Rubin Observatory is set to target $m_{\rm WDM} \sim 18$ keV by probing the subhalo mass function down to masses of $10^6 M_\odot$ through a combination of the effects of subhalos mentioned above [118]; we therefore also show the freeze-in parameters that match the corresponding WDM free-streaming length in Fig. 6. Finally, more futuristic probes of structure formation on small scales could probe free-streaming lengths well beyond these estimates [119]; we show the parameter space that could be accessed with sensitivity to free-streaming lengths at the kpc scale. Overall, the structure formation signatures of this model are manifest in a complementary portion of the parameter space compared to other cosmological probes as well as terrestrial signatures.

We note that DM that decays to a warm lighter state plus relativistic species (like highly boosted electrons) can affect the expansion history of the Universe and potentially alleviate the Hubble and S8 tensions [120–125]. However, decay lifetimes of interest for these tensions are generally comparable to the age of the Universe at recombination. We find that the parameter space that could observably alter the

expansion history is excluded by strong CMB constraints on injected energetic electrons, as shown in Fig. 5.

We additionally note that the presence of the excited state can have an *in situ* impact on the internal dynamics of DM halos after they have already collapsed. Due to the small couplings relevant for freeze-in (and especially the small values of g_χ considered in this work), DM self-scattering is unlikely to be efficient enough for the inelastic nature of the collisions to alter halo properties as in Refs. [126–128]. Meanwhile, the three-body decay of the excited state could impact the halo through the velocity kick imparted to the ground state. The resulting bounds on the decay lifetime are generally comparable to the age of the Universe, ruling out $\tau \lesssim 30$ Gyr under the assumption that the lifetime is sufficiently long to only occur only after halos have formed [129–131]. For this range of lifetimes, the CMB constraints on the injection of energetic electrons already exclude the whole parameter space, as shown in Fig. 5.

VI. DISCUSSION AND CONCLUSIONS

Inelastic freeze-in is a scenario where DM is produced into both ground and excited states by freeze-in via small couplings to the SM. The same couplings that explain the relic abundance can lead to cosmologically long lifetimes for the excited state, with distinct signatures for energy deposition and structure formation once the excited state starts to decay. Inelastic freeze-in thus provides a framework that further motivates cosmological searches for models of late-decaying DM.

In this work, we have explored a model of a pseudo-Dirac fermion coupled to the SM via a kinetically mixed dark photon. we find that in large part of the parameter space there is a long-lived excited state that decays in the late universe. For DM in the mass range ∼30 MeV–TeV with mass splittings above an MeV, we showed that there are complementary probes of this model from accelerator searches for dark photons and cosmological observables. For dark photon couplings accessible with near-future accelerator searches, the primary processes determining the thermal history are the freeze-in production channels $f\bar{f} \to \chi_1\chi_2$ and $Z \to \chi_1\chi_2$, with a negligible amount of scattering through other channels.

If the mass splitting is above ∼1 MeV then the excited state can decay to the ground state plus a pair of electrons (or muons at higher mass splittings). The decays can inject energy into the ambient environment, affecting BBN, CMB spectral distortions and anisotropies, and the Lyman-α forest. We find that the freeze-in mechanism can be realized in a broad region of parameter space that is not excluded by current constraints. We additionally find that much of the currently allowed parameter space would be explored with a future mission like PIXIE. Finally, we explored the possibility of a cosmological signature arising due to the kick imparted to the ground state DM particle during the three-body decay, which could impact structure formation on small cosmological scales that will be probed in the near future.

ACKNOWLEDGMENTS

It is a pleasure to thank Asher Berlin, Nikita Blinov, Xiaoyong Chu, Patrick Foldenauer, Felix Kahlhoefer, Wenzer Qin, and Tracy Slatyer for useful conversations and correspondence pertaining to this work. S. H. acknowledges fellowship funding from the Trottier Space Institute at McGill. S. H. and K. S. acknowledge support from a Natural Sciences and Engineering Research Council of Canada (NSERC) Subatomic Physics Discovery Grant. T. L. acknowledges support from the U.S. Department of Energy under Grant No. DE-SC0022104.

[1] N. Aghanim *et al.* (Planck Collaboration), Planck 2018 results. VI. Cosmological parameters, Astron. Astrophys. **641**, A6 (2020); **652**, C4(E) (2021).
[2] Lawrence J. Hall, Karsten Jedamzik, John March-Russell, and Stephen M. West, Freeze-in production of FIMP dark matter, J. High Energy Phys. 03 (2010) 080.
[3] Xiaoyong Chu, Thomas Hambye, and Michel H. G. Tytgat, The four basic ways of creating dark matter through a portal, J. Cosmol. Astropart. Phys. 05 (2012) 034.
[4] Nicolás Bernal, Matti Heikinheimo, Tommi Tenkanen, Kimmo Tuominen, and Ville Vaskonen, The dawn of FIMP dark matter: A review of models and constraints, Int. J. Mod. Phys. A **32**, 1730023 (2017).
[5] Scott Dodelson and Lawrence M. Widrow, Sterile-neutrinos as dark matter, Phys. Rev. Lett. **72**, 17 (1994).
[6] T. Moroi, H. Murayama, and Masahiro Yamaguchi, Cosmological constraints on the light stable gravitino, Phys. Lett. B **303**, 289 (1993).
[7] John McDonald, Thermally generated gauge singlet scalars as selfinteracting dark matter, Phys. Rev. Lett. **88**, 091304 (2002).
[8] Laura Covi, Leszek Roszkowski, and Michael Small, Effects of squark processes on the axino CDM abundance, J. High Energy Phys. 07 (2002) 023.
[9] Takehiko Asaka, Koji Ishiwata, and Takeo Moroi, Right-handed sneutrino as cold dark matter, Phys. Rev. D **73**, 051301 (2006).

[10] Takehiko Asaka, Koji Ishiwata, and Takeo Moroi, Right-handed sneutrino as cold dark matter of the universe, Phys. Rev. D **75**, 065001 (2007).
[11] Shrihari Gopalakrishna, Andre de Gouvea, and Werner Porod, Right-handed sneutrinos as nonthermal dark matter, J. Cosmol. Astropart. Phys. 05 (2006) 005.
[12] Alexander Kusenko, Sterile neutrinos, dark matter, and the pulsar velocities in models with a Higgs singlet, Phys. Rev. Lett. **97**, 241301 (2006).
[13] Veronique Page, Non-thermal right-handed sneutrino dark matter and the Omega(DM)/Omega(b) problem, J. High Energy Phys. 04 (2007) 021.
[14] Kalliopi Petraki and Alexander Kusenko, Dark-matter sterile neutrinos in models with a gauge singlet in the Higgs sector, Phys. Rev. D **77**, 065014 (2008).
[15] Clifford Cheung, Gilly Elor, and Lawrence J. Hall, The cosmological axino problem, Phys. Rev. D **85**, 015008 (2012).
[16] Clifford Cheung, Gilly Elor, and Lawrence Hall, Gravitino freeze-in, Phys. Rev. D **84**, 115021 (2011).
[17] Xiaoyong Chu, Yann Mambrini, Jérémie Quevillon, and Bryan Zaldivar, Thermal and non-thermal production of dark matter via Z'-portal(s), J. Cosmol. Astropart. Phys. 01 (2014) 034.
[18] Kyu Jung Bae, Howard Baer, Andre Lessa, and Hasan Serce, Coupled Boltzmann computation of mixed axion neutralino dark matter in the SUSY DFSZ axion model, J. Cosmol. Astropart. Phys. 10 (2014) 082.
[19] Christopher Kolda and James Unwin, X-ray lines from R-parity violating decays of keV sparticles, Phys. Rev. D **90**, 023535 (2014).
[20] Bibhushan Shakya, Sterile neutrino dark matter from freeze-in, Mod. Phys. Lett. A **31**, 1630005 (2016).
[21] Angelo Monteux and Chang Sub Shin, Thermal Goldstino production with low reheating temperatures, Phys. Rev. D **92**, 035002 (2015).
[22] Raymond T. Co, Francesco D'Eramo, Lawrence J. Hall, and Duccio Pappadopulo, Freeze-in dark matter with displaced signatures at colliders, J. Cosmol. Astropart. Phys. 12 (2015) 024.
[23] Raymond T. Co, Francesco D'Eramo, and Lawrence J. Hall, Gravitino or axino dark matter with reheat temperature as high as 10^{16} GeV, J. High Energy Phys. 03 (2017) 005.
[24] Karim Benakli, Yifan Chen, Emilian Dudas, and Yann Mambrini, Minimal model of gravitino dark matter, Phys. Rev. D **95**, 095002 (2017).
[25] Pouya Asadi *et al.*, Early-universe model building, arXiv:2203.06680.
[26] Bob Holdom, Two U(1)'s and Epsilon charge shifts, Phys. Lett. **166B**, 196 (1986).
[27] Marco Battaglieri *et al.*, US cosmic visions: New ideas in dark matter 2017: Community report, arXiv:1707.04591.
[28] Simon Knapen, Tongyan Lin, and Kathryn Zurek, Light dark matter: Models and constraints, Phys. Rev. D **96**, 115021 (2017).
[29] Cora Dvorkin, Tongyan Lin, and Katelin Schutz, Making dark matter out of light: Freeze-in from plasma effects, Phys. Rev. D **99**, 115009 (2019).
[30] Cora Dvorkin, Tongyan Lin, and Katelin Schutz, Cosmology of Sub-MeV dark matter freeze-in, Phys. Rev. Lett. **127**, 111301 (2021).
[31] Cora Dvorkin, Kfir Blum, and Marc Kamionkowski, Constraining dark matter-baryon scattering with linear cosmology, Phys. Rev. D **89**, 023519 (2014).
[32] Kimberly K. Boddy, Vera Gluscevic, Vivian Poulin, Ely D. Kovetz, Marc Kamionkowski, and Rennan Barkana, Critical assessment of CMB limits on dark matter-baryon scattering: New treatment of the relative bulk velocity, Phys. Rev. D **98**, 123506 (2018).
[33] David Tucker-Smith and Neal Weiner, Inelastic dark matter, Phys. Rev. D **64**, 043502 (2001).
[34] Douglas P. Finkbeiner and Neal Weiner, Exciting dark matter and the INTEGRAL/SPI 511 keV signal, Phys. Rev. D **76**, 083519 (2007).
[35] Douglas P. Finkbeiner, Nikhil Padmanabhan, and Neal Weiner, CMB and 21-cm signals for dark matter with a long-lived excited state, Phys. Rev. D **78**, 063530 (2008).
[36] Nima Arkani-Hamed, Douglas P. Finkbeiner, Tracy R. Slatyer, and Neal Weiner, A theory of dark matter, Phys. Rev. D **79**, 015014 (2009).
[37] Clifford Cheung, Joshua T. Ruderman, Lian-Tao Wang, and Itay Yavin, Kinetic mixing as the origin of light dark scales, Phys. Rev. D **80**, 035008 (2009).
[38] Fang Chen, James M. Cline, and Andrew R. Frey, Non-Abelian dark matter: Models and constraints, Phys. Rev. D **80**, 083516 (2009).
[39] Brian Batell, Maxim Pospelov, and Adam Ritz, Direct detection of multi-component secluded WIMPs, Phys. Rev. D **79**, 115019 (2009).
[40] Peter W. Graham, Roni Harnik, Surjeet Rajendran, and Prashant Saraswat, Exothermic dark matter, Phys. Rev. D **82**, 063512 (2010).
[41] Masha Baryakhtar, Asher Berlin, Hongwan Liu, and Neal Weiner, Electromagnetic signals of inelastic dark matter scattering, J. High Energy Phys. 06 (2022) 047.
[42] Mariana Carrillo González and Natalia Toro, Cosmology and signals of light pseudo-Dirac dark matter, J. High Energy Phys. 04 (2022) 060.
[43] Jonathan L. Feng and Jordan Smolinsky, Impact of a resonance on thermal targets for invisible dark photon searches, Phys. Rev. D **96**, 095022 (2017).
[44] Patrick J. Fitzpatrick, Hongwan Liu, Tracy R. Slatyer, and Yu-Dai Tsai, New thermal relic targets for inelastic vector-portal dark matter, Phys. Rev. D **106**, 083507 (2022).
[45] Haipeng An and Daneng Yang, Direct detection of freeze-in inelastic dark matter, Phys. Lett. B **818**, 136408 (2021).
[46] E. Aprile *et al.* (XENON Collaboration), Excess electronic recoil events in XENON1T, Phys. Rev. D **102**, 072004 (2020).
[47] E. Aprile *et al.* (XENON Collaboration), Search for new physics in electronic recoil data from XENONnT, Phys. Rev. Lett. **129**, 161805 (2022).
[48] Jared A. Evans, Stefania Gori, and Jessie Shelton, Looking for the WIMP next door, J. High Energy Phys. 02 (2018) 100.

[49] Isaac Hoenig, Gabriel Samach, and David Tucker-Smith, Searching for dilepton resonances below the Z mass at the LHC, Phys. Rev. D **90**, 075016 (2014).
[50] Anastasiia Filimonova, Sam Junius, Laura Lopez Honorez, and Susanne Westhoff, Inelastic Dirac dark matter, J. High Energy Phys. 06 (2022) 048.
[51] Asli M. Abdullahi *et al.*, The present and future status of heavy neutral leptons, J. Phys. G **50**, 020501 (2023).
[52] Michael Duerr, Torben Ferber, Camilo Garcia-Cely, Christopher Hearty, and Kai Schmidt-Hoberg, Long-lived dark Higgs and inelastic dark matter at Belle II, J. High Energy Phys. 04 (2021) 146.
[53] Gilly Elor, Hongwan Liu, Tracy R. Slatyer, and Yotam Soreq, Complementarity for dark sector bound states, Phys. Rev. D **98**, 036015 (2018).
[54] Haipeng An, Maxim Pospelov, and Josef Pradler, New stellar constraints on dark photons, Phys. Lett. B **725**, 190 (2013).
[55] Jae Hyeok Chang, Rouven Essig, and Samuel D. McDermott, Revisiting supernova 1987A constraints on dark photons, J. High Energy Phys. 01 (2017) 107.
[56] Javier Redondo and Marieke Postma, Massive hidden photons as lukewarm dark matter, J. Cosmol. Astropart. Phys. 02 (2009) 005.
[57] Haipeng An, Maxim Pospelov, and Josef Pradler, Dark matter detectors as dark photon helioscopes, Phys. Rev. Lett. **111**, 041302 (2013).
[58] D. Comelli and J. R. Espinosa, Bosonic thermal masses in supersymmetry, Phys. Rev. D **55**, 6253 (1997).
[59] Torsten Bringmann, Saniya Heeba, Felix Kahlhoefer, and Kristian Vangsnes, Freezing-in a hot bath: Resonances, medium effects and phase transitions, J. High Energy Phys. 02 (2022) 110.
[60] Geneviève Bélanger, Fawzi Boudjema, Andreas Goudelis, Alexander Pukhov, and Bryan Zaldivar, micrOMEGAs5.0: Freeze-in, Comput. Phys. Commun. **231**, 173 (2018).
[61] Alexander Belyaev, Neil D. Christensen, and Alexander Pukhov, CALcHEP 3.4 for collider physics within and beyond the Standard Model, Comput. Phys. Commun. **184**, 1729 (2013).
[62] Martin Bauer, Patrick Foldenauer, and Joerg Jaeckel, Hunting all the hidden photons, J. High Energy Phys. 07 (2018) 094.
[63] Prateek Agrawal *et al.*, Feebly-interacting particles: FIPs 2020 workshop report, Eur. Phys. J. C **81**, 1015 (2021).
[64] H. Abreu *et al.* (FASER Collaboration), First results from the search for dark photons with the FASER detector at the LHC, arXiv:2308.05587.
[65] Eder Izaguirre, Gordan Krnjaic, and Brian Shuve, Discovering inelastic thermal-relic dark matter at colliders, Phys. Rev. D **93**, 063523 (2016).
[66] Asher Berlin and Felix Kling, Inelastic dark matter at the LHC lifetime frontier: ATLAS, CMS, LHCb, CODEX-b, FASER, and MATHUSLA, Phys. Rev. D **99**, 015021 (2019).
[67] A. Hayrapetyan *et al.* (CMS Collaboration), Search for inelastic dark matter in events with two displaced muons and missing transverse momentum in proton-proton collisions at $\sqrt{s} = 13$ TeV, arXiv:2305.11649.
[68] Torsten Bringmann and Maxim Pospelov, Novel direct detection constraints on light dark matter, Phys. Rev. Lett. **122**, 171801 (2019).
[69] Nicole F. Bell, James B. Dent, Bhaskar Dutta, Sumit Ghosh, Jason Kumar, Jayden L. Newstead, and Ian M. Shoemaker, Cosmic-ray upscattered inelastic dark matter, Phys. Rev. D **104**, 076020 (2021).
[70] Mathias Garny, Jan Heisig, Benedikt Lülf, and Stefan Vogl, Coannihilation without chemical equilibrium, Phys. Rev. D **96**, 103521 (2017).
[71] Katelin Schutz and Tracy R. Slatyer, Self-scattering for dark matter with an excited state, J. Cosmol. Astropart. Phys. 01 (2015) 021.
[72] Tracy R. Slatyer, Indirect dark matter signatures in the cosmic dark ages. I. Generalizing the bound on s-wave dark matter annihilation from Planck results, Phys. Rev. D **93**, 023527 (2016).
[73] Hitoshi Murayama, Notes on Phase Space, http://hitoshi.berkeley.edu/233B/phasespace.
[74] Steven R. Furlanetto, S. Peng Oh, and Elena Pierpaoli, The effects of dark matter decay and annihilation on the High-Redshift 21 cm background, Phys. Rev. D **74**, 103502 (2006).
[75] Carmelo Evoli, Andrei Mesinger, and Andrea Ferrara, Unveiling the nature of dark matter with high redshift 21 cm line experiments, J. Cosmol. Astropart. Phys. 11 (2014) 024.
[76] Hongwan Liu and Tracy R. Slatyer, Implications of a 21-cm signal for dark matter annihilation and decay, Phys. Rev. D **98**, 023501 (2018).
[77] Masahiro Kawasaki, Kazunori Kohri, and Takeo Moroi, Big-bang nucleosynthesis and hadronic decay of long-lived massive particles, Phys. Rev. D **71**, 083502 (2005).
[78] Vivian Poulin and Pasquale Dario Serpico, Nonuniversal BBN bounds on electromagnetically decaying particles, Phys. Rev. D **91**, 103007 (2015).
[79] Vivian Poulin, Julien Lesgourgues, and Pasquale D. Serpico, Cosmological constraints on exotic injection of electromagnetic energy, J. Cosmol. Astropart. Phys. 03 (2017) 043.
[80] Lindsay Forestell, David E. Morrissey, and Graham White, Limits from BBN on light electromagnetic decays, J. High Energy Phys. 01 (2019) 074.
[81] J. Chluba and R. A. Sunyaev, The evolution of CMB spectral distortions in the early Universe, Mon. Not. R. Astron. Soc. **419**, 1294 (2012).
[82] Matteo Lucca, Nils Schöneberg, Deanna C. Hooper, Julien Lesgourgues, and Jens Chluba, The synergy between CMB spectral distortions and anisotropies, J. Cosmol. Astropart. Phys. 02 (2020) 026.
[83] Tracy R. Slatyer, Energy injection and absorption in the cosmic dark ages, Phys. Rev. D **87**, 123513 (2013).
[84] Hongwan Liu, Gregory W. Ridgway, and Tracy R. Slatyer, Code package for calculating modified cosmic ionization and thermal histories with dark matter and other exotic energy injections, Phys. Rev. D **101**, 023530 (2020).
[85] Patrick Stöcker, Michael Krämer, Julien Lesgourgues, and Vivian Poulin, Exotic energy injection with ExoCLASS:

Application to the Higgs portal model and evaporating black holes, J. Cosmol. Astropart. Phys. 03 (2018) 018.
[86] D. J. Fixsen, E. S. Cheng, J. M. Gales, John C. Mather, R. A. Shafer, and E. L. Wright, The Cosmic Microwave Background spectrum from the full COBE FIRAS data set, Astrophys. J. **473**, 576 (1996).
[87] Federico Bianchini and Giulio Fabbian, CMB spectral distortions revisited: A new take on μ distortions and primordial non-Gaussianities from FIRAS data, Phys. Rev. D **106**, 063527 (2022).
[88] Jens Chluba and Donghui Jeong, Teasing bits of information out of the CMB energy spectrum, Mon. Not. R. Astron. Soc. **438**, 2065 (2014).
[89] A. Kogut *et al.*, The Primordial Inflation Explorer (PIXIE): A nulling polarimeter for cosmic microwave background observations, J. Cosmol. Astropart. Phys. 07 (2011) 025.
[90] Tracy R. Slatyer and Chih-Liang Wu, General constraints on dark matter decay from the cosmic microwave background, Phys. Rev. D **95**, 023010 (2017).
[91] Hongwan Liu, Wenzer Qin, Gregory W. Ridgway, and Tracy R. Slatyer, Lyman-α constraints on cosmic heating from dark matter annihilation and decay, Phys. Rev. D **104**, 043514 (2021).
[92] Rouven Essig, Eric Kuflik, Samuel D. McDermott, Tomer Volansky, and Kathryn M. Zurek, Constraining light dark matter with diffuse X-ray and gamma-ray observations, J. High Energy Phys. 11 (2013) 193.
[93] Timothy Cohen, Kohta Murase, Nicholas L. Rodd, Benjamin R. Safdi, and Yotam Soreq, γ-ray constraints on decaying dark matter and implications for IceCube, Phys. Rev. Lett. **119**, 021102 (2017).
[94] Andrea Massari, Eder Izaguirre, Rouven Essig, Andrea Albert, Elliott Bloom, and Germán Arturo Gómez-Vargas, Strong optimized conservative Fermi-LAT constraints on dark matter models from the inclusive photon spectrum, Phys. Rev. D **91**, 083539 (2015).
[95] Marco Cirelli, Nicolao Fornengo, Jordan Koechler, Elena Pinetti, and Brandon M. Roach, Putting all the X in one basket: Updated X-ray constraints on sub-GeV dark matter, J. Cosmol. Astropart. Phys. 07 (2023) 026.
[96] A. C. Cummings, E. C. Stone, B. C. Heikkila, N. Lal, W. R. Webber, G. Jóhannesson, I. V. Moskalenko, E. Orlando, and T. A. Porter, Galactic cosmic rays in the local interstellar medium: Voyager 1 Observations and model results, Astrophys. J. **831**, 18 (2016).
[97] Mathieu Boudaud, Julien Lavalle, and Pierre Salati, Novel cosmic-ray electron and positron constraints on MeV dark matter particles, Phys. Rev. Lett. **119**, 021103 (2017).
[98] Mei-Yu Wang and Andrew R. Zentner, Effects of unstable dark matter on large-scale structure and constraints from future surveys, Phys. Rev. D **85**, 043514 (2012).
[99] Mei-Yu Wang, Rupert A. C. Croft, Annika H. G. Peter, Andrew R. Zentner, and Chris W. Purcell, Lyman-α forest constraints on decaying dark matter, Phys. Rev. D **88**, 123515 (2013).
[100] Paul Bode, Jeremiah P Ostriker, and Neil Turok, Halo formation in warm dark matter models, Astrophys. J. **556**, 93 (2001).
[101] Matteo Viel, Julien Lesgourgues, Martin G Haehnelt, Sabino Matarrese, and Antonio Riotto, Constraining warm dark matter candidates including sterile neutrinos and light gravitinos with WMAP and the Lyman-α forest, Phys. Rev. D **71**, 063534 (2005).
[102] Aurel Schneider, Robert E. Smith, Andrea V. Maccio, and Ben Moore, Nonlinear evolution of cosmological structures in warm dark matter models, Mon. Not. R. Astron. Soc. **424**, 684 (2012).
[103] Vid Iršič *et al.*, New Constraints on the free-streaming of warm dark matter from intermediate and small scale Lyman-α forest data, Phys. Rev. D **96**, 023522 (2017).
[104] Riccardo Murgia, Vid Iršič, and Matteo Viel, Novel constraints on noncold, nonthermal dark matter from Lyman- α forest data, Phys. Rev. D **98**, 083540 (2018).
[105] Keir K. Rogers and Hiranya V. Peiris, Strong bound on canonical ultralight axion dark matter from the Lyman-Alpha forest, Phys. Rev. Lett. **126**, 071302 (2021).
[106] Ethan O. Nadler, Vera Gluscevic, Kimberly K. Boddy, and Risa H. Wechsler, Constraints on dark matter microphysics from the milky way satellite population, Astrophys. J. **878**, L32 (2019); **878**, 32 (2019).
[107] E. O. Nadler *et al.* (DES Collaboration), Milky way satellite census. III. Constraints on dark matter properties from observations of milky way satellite galaxies, Phys. Rev. Lett. **126**, 091101 (2021).
[108] Jen-Wei Hsueh, Wolfgang Enzi, Simona Vegetti, MW Auger, Christopher D Fassnacht, Giulia Despali, Leon VE Koopmans, and John P McKean, Sharp–VII. New constraints on the dark matter free-streaming properties and substructure abundance from gravitationally lensed quasars, Mon. Not. R. Astron. Soc. **492**, 3047 (2020).
[109] Daniel Gilman, Simon Birrer, Anna Nierenberg, Tommaso Treu, Xiaolong Du, and Andrew Benson, Warm dark matter chills out: Constraints on the halo mass function and the free-streaming length of dark matter with eight quadruple-image strong gravitational lenses, Mon. Not. R. Astron. Soc. **491**, 6077 (2020).
[110] Nilanjan Banik, Jo Bovy, Gianfranco Bertone, Denis Erkal, and T. J. L. de Boer, Evidence of a population of dark subhaloes from Gaia and Pan-STARRS observations of the GD-1 stream, Mon. Not. R. Astron. Soc. **502**, 2364 (2021).
[111] Nilanjan Banik, Jo Bovy, Gianfranco Bertone, Denis Erkal, and T. J. L. de Boer, Novel constraints on the particle nature of dark matter from stellar streams, J. Cosmol. Astropart. Phys. 10 (2021) 043.
[112] Julian B. Muñoz, Cora Dvorkin, and Francis-Yan Cyr-Racine, Probing the small-scale matter power spectrum with large-scale 21-cm data, Phys. Rev. D **101**, 063526 (2020).
[113] Wolfgang Enzi *et al.*, Joint constraints on thermal relic dark matter from strong gravitational lensing, the Ly α forest, and Milky Way satellites, Mon. Not. R. Astron. Soc. **506**, 5848 (2021).
[114] Ethan O. Nadler, Simon Birrer, Daniel Gilman, Risa H. Wechsler, Xiaolong Du, Andrew Benson, Anna M. Nierenberg, and Tommaso Treu, Dark matter constraints from a unified analysis of strong gravitational lenses and Milky Way satellite galaxies, Astrophys. J. **917**, 7 (2021).
[115] Julien Baur, Nathalie Palanque-Delabrouille, Christophe Yeche, Alexey Boyarsky, Oleg Ruchayskiy, Éric

Armengaud, and Julien Lesgourgues, Constraints from Ly-α forests on non-thermal dark matter including resonantly-produced sterile neutrinos, J. Cosmol. Astropart. Phys. 12 (2017) 013.

[116] G. Parimbelli, G. Scelfo, S. K. Giri, A. Schneider, M. Archidiacono, S. Camera, and M. Viel, Mixed dark matter: Matter power spectrum and halo mass function, J. Cosmol. Astropart. Phys. 12 (2021) 044.

[117] Deanna C. Hooper, Nils Schöneberg, Riccardo Murgia, Maria Archidiacono, Julien Lesgourgues, and Matteo Viel, One likelihood to bind them all: Lyman-α constraints on non-standard dark matter, J. Cosmol. Astropart. Phys. 10 (2022) 032.

[118] Alex Drlica-Wagner *et al.* (LSST Dark Matter Group Collaboration), Probing the fundamental nature of dark matter with the large synoptic survey telescope, arXiv: 1902.01055.

[119] Keith Bechtol *et al.*, Snowmass2021 Cosmic Frontier White Paper: Dark matter physics from halo measurements, in 2022 Snowmass Summer Study (2022), arXiv: 2203.07354.

[120] Gordon Blackadder and Savvas M. Koushiappas, Cosmological constraints to dark matter with two- and many-body decays, Phys. Rev. D **93**, 023510 (2016).

[121] Kyriakos Vattis, Savvas M. Koushiappas, and Abraham Loeb, Dark matter decaying in the late Universe can relieve the H0 tension, Phys. Rev. D **99**, 121302 (2019).

[122] Balakrishna S. Haridasu and Matteo Viel, Late-time decaying dark matter: Constraints and implications for the H_0-tension, Mon. Not. R. Astron. Soc. **497**, 1757 (2020).

[123] Guillermo Franco Abellán, Riccardo Murgia, Vivian Poulin, and Julien Lavalle, Implications of the S_8 tension for decaying dark matter with warm decay products, Phys. Rev. D **105**, 063525 (2022).

[124] Guillermo Franco Abellán, Riccardo Murgia, and Vivian Poulin, Linear cosmological constraints on two-body decaying dark matter scenarios and the S8 tension, Phys. Rev. D **104**, 123533 (2021).

[125] Lea Fuß and Mathias Garny, Decaying dark matter and Lyman-α forest constraints, J. Cosmol. Astropart. Phys. 10 (2023) 020.

[126] Mark Vogelsberger, Jesús Zavala, Katelin Schutz, and Tracy R. Slatyer, Evaporating the Milky Way halo and its satellites with inelastic self-interacting dark matter, Mon. Not. R. Astron. Soc. **484**, 5437 (2019).

[127] Kun Ting Eddie Chua, Karia Dibert, Mark Vogelsberger, and Jesús Zavala, The impact of inelastic self-interacting dark matter on the dark matter structure of a Milky Way halo, Mon. Not. R. Astron. Soc. **500**, 1531 (2020).

[128] Stephanie O'Neil *et al.*, Endothermic self-interacting dark matter in milky way-like dark matter haloes, Mon. Not. R. Astron. Soc. **524**, 288 (2023).

[129] Annika H. G. Peter, Christopher E. Moody, and Marc Kamionkowski, Dark-matter decays and self-gravitating halos, Phys. Rev. D **81**, 103501 (2010).

[130] Mei-Yu Wang, Annika H. G. Peter, Louis E. Strigari, Andrew R. Zentner, Bryan Arant, Shea Garrison-Kimmel, and Miguel Rocha, Cosmological simulations of decaying dark matter: Implications for small-scale structure of dark matter haloes, Mon. Not. R. Astron. Soc. **445**, 614 (2014).

[131] S. Mau *et al.* (DES Collaboration), Milky way satellite census. IV. Constraints on decaying dark matter from observations of milky way satellite galaxies, Astrophys. J. **932**, 128 (2022).